Monthly Notices of the ROYAL ASTRONOMICAL SOCIETY

MNRAS **527,** 7701–7712 (2024) https://doi.org/10.1093/mnras/stad3730
Advance Access publication 2023 December 04

Neutrinos from pre-supernova in the framework of TQRPA method

A. A. Dzhioev,[1]★ A. V. Yudin,[2,3]★ N. V. Dunina-Barkovskaya[2] and A. I. Vdovin[1]

[1]*Bogoliubov Laboratory of Theoretical Physics, Joint Institute for Nuclear Research, 141980 Dubna, Russia*
[2]*National Research Center Kurchatov Institute, pl. Kurchatova 1, Moscow 123182, Russia*
[3]*Novosibirsk State University, Pirogova, 2, 630090 Novosibirsk, Russia*

Accepted 2023 November 30. Received 2023 November 30; in original form 2023 September 7

ABSTRACT

We propose a new method for calculating spectra and luminosities for (anti)neutrinos produced in the pre-supernova environment by weak processes with hot nuclei. It is based on the thermal quasiparticle random phase approximation (TQRPA), which allows microscopic thermodynamically consistent calculations of the weak interaction response of nuclei at finite temperatures. For realistic representative pre-supernova conditions from the stellar evolution code MESA, we compute (anti)neutrino luminosities and spectra arising from neutral- and charged-current weak reactions with hot ^{56}Fe and compare them with the contribution of thermal processes. We find that the TQRPA approach produces not only a higher total luminosity of electron neutrinos (mainly born in the electron capture reaction), compared to the standard technique based on the large-scale shell model (LSSM) weak interaction rates, but also a harder neutrino spectrum. Besides, applying the TQRPA and LSSM, we find that in the context of electron antineutrino generation, the neutral-current nuclear de-excitation (ND) process via neutrino-antineutrino pair emission is at least as important as the electron–positron pair annihilation process. We also show that flavour oscillations enhance the high-energy contribution of the ND process to the electron antineutrino flux. This could potentially be important for pre-supernova antineutrino registration by the Earth's detectors.

Key words: neutrinos – instrumentation: detectors – supernovae: general.

1 INTRODUCTION

Supernova explosions are magnificent and not yet fully understood phenomena of nature. For dozens of days, the dying star shines like an entire host galaxy. But despite this, in massive stars that end their lives as a core-collapse supernova, the main amount of energy during the explosion (of an order of a few 10^{53} erg) is lost by neutrinos. The first and so far the only detection of neutrinos from a supernova occurred on 1987, February 23; it was a famous supernova SN1987A that flared up in the Large Magellanic Cloud (see e.g. Alekseev et al. 1987; Bionta et al. 1987; Hirata et al. 1987; Ryazhskaya 2006).

But even before the explosion, neutrino plays an important role in the life of a massive star: already at the stage of the neon–oxygen core (a few years before the collapse), the neutrino luminosity becomes higher than the photon luminosity (Weaver, Zimmerman & Woosley 1978), and just before the collapse, the energy loss via neutrino emission is many orders of magnitude superior to other processes (Kato et al. 2017). Such a star, called a pre-supernova, appears to be a promising source of neutrinos to be detected (Odrzywolek, Misiaszek & Kutschera 2004b; Patton et al. 2017b). Pre-supernova (anti)neutrinos, if registered, can serve as an alarm signal for an upcoming explosion (Kutschera, Odrzywołek & Misiaszek 2009). Moreover, since neutrinos can freely propagate through the stellar matter, they carry direct information about thermodynamic conditions in the core and their observation would offer a possibility for studying the physical processes that lead to the core collapse.

Neutrino emission in a stellar core occurs due to a number of thermal processes and nuclear weak reactions. Thermal neutrinos are mostly emitted via the electron–positron pair annihilation and plasmon decay, and their production is entirely determined by the core temperature, density, and electron fraction (Itoh et al. 1996; Kato et al. 2015). In contrast, neutrino emission via nuclear weak reactions, such as $\beta^{\pm}$-decay and $e^{\pm}$-capture, has a stronger dependence on the isotopic composition of the core and its study therefore requires realistic stellar evolution simulations with a large and accurate nuclear reaction network (Odrzywolek & Heger 2010). However, not only isotopic composition but also thermodynamic conditions in the core affect the neutrino production in nuclear weak reactions. The reason is that nuclear excited states are thermally populated in the high-temperature stellar environment, and weak reactions on thermally excited states allow the emission of neutrinos with rather high energy. The relative contribution of these high-energy neutrinos to the total flux depends on temperature. It is important to realize that despite the Boltzmann suppression, the gain in phase space combined with the large matrix element and increased density of thermally excited states can make this contribution significant. Eventually, the balance between all these factors depends on thermodynamic conditions and properties of individual nuclei.

In Patton, Lunardini & Farmer (2017a); Patton et al. (2017b), the contribution of charged-current nuclear weak processes to neutrino emissivities was analysed for different realistic thermodynamic

★ E-mail: dzhioev@theor.jinr.ru (AAD); yudin@itep.ru (AVY)

conditions and isotopic compositions of the star obtained from the state-of-the-art stellar evolution code MESA. It was found that, under certain conditions, nuclear processes compete with thermal processes in their contribution to the (anti)neutrino flux or even dominate in the energy window relevant for detection, which is mostly due to the decay and electron capture on *pf*-shell nuclei with $A = 50$–60 (iron-group nuclei). However, it was pointed out that while total emissivities are relatively robust, the high-energy tails of the neutrino spectra in the detectable window are very sensitive to the details of the calculations. Specifically, the source of the error lies in the so called single-strength (or effective q-value) approximation (Langanke, Martínez-Pinedo & Sampaio 2001), which was adopted in Patton, Lunardini & Farmer (2017a); Patton et al. (2017b) to generate charged-current neutrino spectra. An exploratory study of this error was performed in Misch & Fuller (2016), and it was shown that the specific neutrino energy spectrum obtained from the single-strength approximation could miss important features when the most important weak transitions involve thermally excited states.

In Misch & Fuller (2016), (anti)neutrino emission via charged-current reactions was considered using some *sd*-shell nuclei as an example. To do this, shell-model calculations were preformed to obtain strength distributions of Gamow–Teller and Fermi transitions, which dominate nuclear weak reactions at pre-supernova conditions. However, for *pf*-shell nuclei, large-scale shell-model (LSSM) calculations of the GT strength distributions require a huge dimension of the model space, and therefore they are still limited by the nuclear ground and low-lying excited states (Caurier et al. 2005). When performing shell-model calculations of stellar weak-interaction rates, this issue is overcome by employing the Brink hypothesis and the method of 'back-resonances' (Langanke & Martínez-Pinedo 2000). However, even if we could perform precise LSSM calculations for highly excited states, the state-by-state consideration of individual contributions would remain computationally infeasible because of too many thermally populated states at pre-supernova temperatures $T \approx 1\,\mathrm{MeV}$ ($10^{10}\,\mathrm{K} = 0.86\,\mathrm{MeV}$).

To avoid these shortcomings and compute stellar weak-interaction rates for hot thermally excited nuclei in a microscopic, thermodynamically consistent way, the thermal quasiparticle random-phase approximation (TQRPA) was proposed in Dzhioev et al. (2010). The TQRPA approach is based on a statistical description of the hot nucleus, and it enables one to obtain temperature-dependent strength functions for nuclear transitions involved in the considered weak reaction. The advantage of the TQRPA is that it makes it possible to treat both endoergic and exoergic weak processes without application of the Brink hypothesis and the 'back-resonance' method and without violation of the detailed balance principle. Later on, the combination of the TQRPA and the Skyrme energy density functional methods was successfully applied to study both charged-current (Dzhioev, Vdovin & Stoyanov 2019; Dzhioev et al. 2020) and neutral-current (Dzhioev et al. 2016; Kondratyev et al. 2019) stellar weak reactions with *pf*-shell and heavier neutron-rich nuclei (see also recent reviews Dzhioev & Vdovin (2022a, b, c)).

In our recent paper, Dzhioev et al. (2023), the TQRPA method was applied for the first time for computing (anti)neutrino spectrum and energy loss rates due to nuclear weak processes under specific pre-supernova conditions, which correspond to a realistic pre-supernova model. Using the hot ^{56}Fe as an example, we have shown that thermodynamically consistent TQRPA calculations predict an electron-neutrino spectrum with an enhanced high-energy fraction. These high-energy neutrinos are emitted via the exoergic electron capture, i.e. the process when a thermally excited hot nucleus captures an electron and then de-excites by energy transfer to the emitted neutrino. Another interesting process considered in Dzhioev et al. (2023) is the de-excitation of a hot nucleus via the neutrino-antineutrino pair emission. This neutral-current process produces $\nu\bar{\nu}$-pairs of all flavours with equal probability and its potential importance for production of high-energy pre-supernova (anti)neutrinos was outlined in (Misch & Fuller 2016; Patton et al. 2017b). In Dzhioev et al. (2023), performing TQRPA calculations for both charged- and neutral-current weak-interaction processes with ^{56}Fe generating electron (anti)neutrinos, we have shown that $\nu\bar{\nu}$-pair emission has practically no effect on the ν_e spectrum, while this process produces more high-energy electron antineutrinos than other nuclear weak processes (positron capture and β^--decay).

We would also like to mention that to date the only study analysing the impact of $\nu\bar{\nu}$-pair emission from nuclear de-excitation on core-collapse supernova simulations has been performed by Fischer, Langanke & Martínez-Pinedo (2013). In particular, this study showed that $\nu\bar{\nu}$-pair emission has basically no impact on the global supernova properties and the energy loss during collapse is dominated by electron neutrinos produced by electron captures on nuclei. However, it was found that nuclear de-excitation is the leading source for the production of electron antineutrinos as well as (μ, τ) (anti)neutrinos during the collapse phase.

In Dzhioev et al. (2023), (anti)neutrino spectra and energy loss rates due to nuclear processes were computed at sample points inside the stellar core just before the onset of the collapse. At this moment, for the considered pre-supernova model, the iron isotope ^{56}Fe dominates the isotopic composition of the central part of the stellar core. The present work extends our previous study, and here we apply the TQRPA method at the same pre-supernova conditions to calculate total (anti)neutrino spectra and luminosities generated in different nuclear weak processes and integrated over the volume of emission. In this paper, we also compute (anti)neutrino spectra and luminosities from thermal processes and take into account oscillation effects.

Our paper is organized as follows: in the next section, we briefly outline the TQRPA method for computing neutrino spectra produced by hot nuclei in stellar interior. A comprehensive description of the TQRPA and its application to study stellar weak-interaction processes is given in the recent reviews (Dzhioev & Vdovin 2022a, b, c). Then in Section 3, we describe the structure of a particular pre-supernova model, which has been used to explore the role of weak nuclear processes in (anti)neutrino production. In Section 4, taking into account both nuclear and thermal processes, we calculate the luminosities of different (anti)neutrino flavours inside the star and corresponding spectra. After that in Section 5, we compare the properties of (anti)neutrino spectra obtained in the framework of the TQRPA with those obtained using a more conventional method based on the LSSM calculations and the effective q-value approximation. Before proceeding to a discussion of the detectability of the calculated antineutrino fluxes (see Section 7) in Section 6, we consider the issue of neutrino oscillation effects. Finally, we provide a short 'Summary and Perspectives' section.

2 TQRPA METHOD

In what follows, we assume that under the pre-supernova conditions we are concerned, weak processes with *pf*-shell nuclei are dominated by Gamow–Teller transitions and the emitted (anti)neutrinos freely leave the star. Then, the (anti)neutrino spectra for a single hot nucleus can be expressed in terms of the temperature-dependent GT strength functions:

(i) electron (EC) or positron (PC) capture

$$\phi^{\rm EC,PC}(E_\nu) = \frac{G_{\rm F}^2 V_{\rm ud}^2 (g_A^*)^2}{2\pi^3\hbar^7 c^6} E_\nu^2 \times \int_{-E_\nu+m_{\rm e}c^2}^{+\infty} S_{\rm GT_\pm}(E,T) E_{\rm e} p_{\rm e} c f_{e^\mp}(E_{\rm e}) F(\pm Z, E_{\rm e})\,{\rm d}E, \quad (1)$$

where the upper (lower) sign corresponds to EC (PC) and $E_{\rm e} = E_\nu + E$, $p_{\rm e}c = (E_{\rm e}^2 - m_{\rm e}^2c^4)^{1/2}$;

(ii) $\beta^\mp$-decay

$$\phi^{\beta^\mp}(E_\nu) = \frac{G_{\rm F}^2 V_{\rm ud}^2 (g_A^*)^2}{2\pi^3\hbar^7 c^6} E_\nu^2 \times \int_{-\infty}^{-E_\nu-m_{\rm e}c^2} S_{\rm GT_\mp}(E,T) E_{\rm e} p_{\rm e} c (1 - f_{e^\mp}(E_{\rm e})) F(\pm Z+1, E_{\rm e})\,{\rm d}E, \quad (2)$$

where the upper (lower) sign corresponds to the β^-- (β^+-) decay and $E_{\rm e} = -E_\nu - E$;

(iii) $\nu\bar{\nu}$-pair emission via nuclear de-excitation (ND)

$$\phi^{\rm ND}(E_\nu) = \frac{G_{\rm F}^2 g_A^2}{2\pi^3\hbar^7 c^6} E_\nu^2 \int_{-\infty}^{E_\nu} S_{\rm GT_0}(E,T)(E+E_\nu)^2\,{\rm d}E. \quad (3)$$

Note that the ND process produces the same spectra for $\nu_{\rm e}$ and $\bar{\nu}_{\rm e}$. Moreover, the spectrum of other (anti)neutrino flavours is also given by (3).

In the above expressions, $G_{\rm F}$ denotes the Fermi coupling constant, $V_{\rm ud}$ is the up-down element of the Cabibbo–Kobayashi–Maskava quark-mixing matrix, and $g_{\rm A} = -1.27$ is the weak axial coupling constant. Note that for charged-current reactions, we use the effective coupling constant $g_{\rm A}^*$ that takes into account the experimentally observed quenching of the GT$_\pm$ strength. The function $f_{e^-(e^+)}(E)$ is the Fermi–Dirac distribution for electrons (positrons), which depends on the chemical potential μ_{e^-} ($\mu_{e^+} = -\mu_{e^-}$) and temperature T, and the Fermi function $F(Z, E)$ takes into account the distortion of the charged lepton wave function by the Coulomb field of the nucleus.

The presented expressions for $\phi^i(E_\nu)$ (i = EC,PC,ND, $\beta^\pm$) are exact in the sense that no additional assumptions or approximations are made in their derivation. Approximations should be made for computing the temperature-dependent GT strength functions defined as

$$S_{\rm GT_{\pm,0}}(E,T) = \sum_{i,f} p_i(T) B_{if}^{(\pm,0)} \delta(E - E_{if}). \quad (4)$$

Here, $p_i(T) = {\rm e}^{-E_i/kT}/Z(T)$ is the Boltzmann population factor for a state i in the parent nucleus, $B_{if}^{\pm,0} = |\langle f\|{\rm GT}_{\pm,0}\|i\rangle|^2/(2J_i+1)$ is the reduced transition probability (transition strength) from the state i to the state f in the daughter nucleus; ${\rm GT}_0 = \vec{\sigma}\,t_0$ for neutral-current reactions and ${\rm GT}_\mp = \vec{\sigma}\,t_\pm$ for charged-current reactions.[1]; E_{if} is the transition energy between the initial and final states, and it can be both positive and negative. The pre-supernova model considered in this study has typical temperatures inside the star around $T_9 \approx 1$–10 (see the discussion below). Obviously, at such high temperatures, an explicit state-by-state evaluation of the sums in equation (4) is impossible with current nuclear models. We compute the temperature-dependent strength function (4) applying the TQRPA approach, which is a technique based on the quasiparticle random phase approximation extended to the finite temperature by the superoperator formalism in the Liouville space (Dzhioev & Vdovin 2022a).

The central concept of the TQRPA is the thermal vacuum $|0(T)\rangle$, a pure state in the Liouville space, which corresponds to the grand canonical density matrix operator for a hot nucleus. The time-translation operator in the Liouville space is the so-called thermal Hamiltonian $\mathcal{H}$ constructed from the nuclear Hamiltonian after introducing the particle creation and annihilation superoperators. Within the TQRPA, the strength function (4) is expressed in terms of the transition matrix elements from the thermal vacuum to the eigenstates (thermal phonons) of the thermal Hamiltonian $\mathcal{H}|Q_i\rangle = \omega_i|Q_i\rangle$:

$$S_{\rm GT_{\pm,0}}(E,T) = \sum_i \mathcal{B}_i^{(\pm,0)} \delta(E - \omega_i \mp \Delta_{\rm np}). \quad (5)$$

Here, $\mathcal{B}_i^{(\pm,0)} = |\langle Q_i\|{\rm GT}_{\pm,0}\|0(T)\rangle|^2$ is the transition strength to the ith thermal phonon state of a hot nucleus and $E_i^{(\pm,0)} = \omega_i \pm \Delta_{\rm np}$ is the respective transition energy; $\Delta_{\rm np} = 0$ for charge-neutral transitions, while for charge-exchange transitions $\Delta_{\rm np} = \delta\lambda_{\rm np} + \delta M_{\rm np}$, where $\delta\lambda_{\rm np} = \lambda_{\rm n} - \lambda_{\rm p}$ is the difference between neutron and proton chemical potentials in the nucleus, and $\delta M_{\rm np} = 1.293$ MeV is the neutron–proton mass splitting. Note that eigenvalues of the thermal Hamiltonian, ω_i, can be both positive and negative. As a result, the strength functions (5) for upward ($E > 0$) and downward ($E < 0$) transitions obey the detailed balance principle:

$$S_{\rm GT_0}(-E,T) = {\rm e}^{-E/kT} S_{\rm GT_0}(E,T) \quad (6)$$

for charge-neutral GT transitions, and

$$S_{\rm GT_\mp}(-E,T) = {\rm e}^{-(E\mp\Delta_{np})/kT} S_{\rm GT_\pm}(E,T) \quad (7)$$

for charge-exchange GT transitions. This property makes the TQRPA approach thermodynamically consistent. Due to negative-energy downward GT transitions, the $\beta^\pm$-decay and $\nu\bar{\nu}$-pair emission become possible for hot nuclei, which are stable in their ground-state. Moreover, due to enhanced phase space such negative-energy transitions may dominate the EC and PC processes.

In Dzhioev et al. (2023), (anti)neutrino spectra due to weak processes with hot ^{56}Fe were computed applying self-consistent TQRPA calculations based on the SkM* parametrization of the Skyrme effective nucleon–nucleon interaction. Here, 'self-consistent' means that both the mean field for protons and neutrons and the residual interaction are obtained from the same energy density functional. In the present study, we also use the SkM* parametrization. To take into account the quenching of the GT$_\pm$ strength in ^{56}Fe, we use the effective coupling constant $g_A^* = 0.56 g_A$. Then, the total GT$_\pm$ strength in ^{56}Fe at $T = 0$ becomes close to the experimental one and to the LSSM results (Caurier et al. 1999).

Before proceeding further, let us briefly recall the main results obtained in Dzhioev et al. (2023):

(i) Considering the temperature evolution of the GT strength functions in ^{56}Fe, we have shown that the TQRPA does not support the Brink hypothesis, and under relevant pre-supernova conditions, the thermal population of nuclear excited states makes possible (unblocks) negative- and low-energy GT transitions whose strength increases with temperature. Negative-energy downward transitions contribute to exoergic weak reactions with hot nuclei.

(ii) Calculated electron neutrino spectra confirm the conclusion of Langanke, Martínez-Pinedo & Sampaio (2001) that the effective q-value approximation can be applied under stellar conditions with the electron chemical potential high enough to allow the excitation of the GT$_+$ resonance by electron capture. Such conditions occur during

[1]The zero component of the isospin operator is denoted by t_0, while t_- and t_+ are the isospin-lowering ($t_-|n\rangle = |p\rangle$) and isospin-rising ($t_+|p\rangle = |n\rangle$) operators.

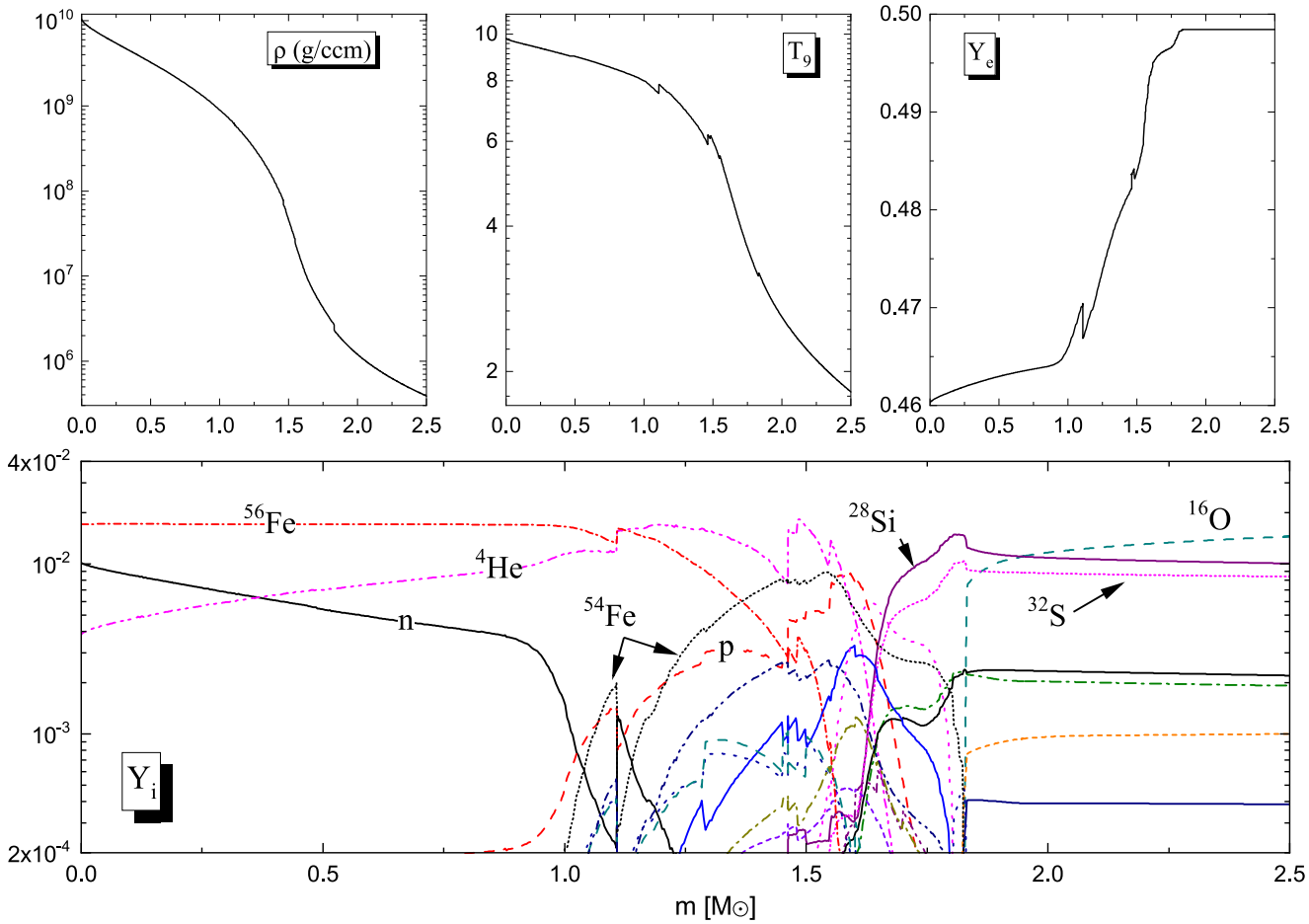

Figure 1. Top panels: density ρ, temperature T_9, and electron fraction Y_e profiles along the mass coordinate m for the `25_79_0p005_ml` pre-supernova model at the onset of the core collapse. Bottom panel: the chemical composition at the same conditions.

the collapse phase. However, our calculations clearly demonstrate that this approximation can fail in the pre-supernova phase when negative-energy GT_+ transitions from thermally excited states noticeably contribute to electron capture and the resulting neutrino energy spectrum is double-peaked. On the whole, thermodynamically consistent calculations of the electron-neutrino spectra performed without assuming the Brink hypothesis indicate that thermal effects on the GT_+ strength function shift the spectrum to higher energies, and thus make ν_e neutrino detection more likely.

(iii) The inclusion into consideration of the $\nu\bar{\nu}$-pair emission by hot nuclei shows that this neutral-current process might be a dominant source of high-energy ($E_{\bar{\nu}} \approx 5$–10 MeV) $\bar{\nu}_e$ and (μ, τ) (anti)neutrinos emitted via de-excitation of the GT_0 resonance. Moreover, since the ND process is entirely independent of the electron density and only depends on temperature, the detection of high-energy pre-supernova antineutrinos might be a test for thermodynamic conditions in the stellar interior.

3 PRE-SN STRUCTURE

Let us now consider a characteristic structure of the pre-supernova model we use in the present work. As in our previous study Dzhioev et al. (2023), we use the model `25_79_0p005_ml` from Farmer et al. (2016), which is a realistic pre-supernova model with a good mass resolution and the central temperature which is high enough for our estimates. Its name means that the initial mass of the model was $25\,M_\odot$, the nuclear reaction network was `mesa-79.net`, the maximum mass of a computational cell was $0.005\,M_\odot$, and the mass loss during the stellar evolution was taken into account (for more details see Farmer et al. 2016). The authors of Farmer et al. (2016) employ the stellar evolution code MESA (Paxton et al. 2015), version 7624. In the output, MESA produces time-evolving profiles of mass density, temperature, electron fraction Y_e, and chemical composition as a function of the mass coordinate. The profile that we use corresponds to the onset of the core collapse, which is defined as the time when the infall velocity exceeds $1000\,\mathrm{km\,s^{-1}}$ anywhere in the star.

The detailed structure of this profile is given in Fig. 1. Three top panels show the density ρ, temperature $T_9 \equiv T/10^9$ K, and the electron fraction Y_e as a function of the mass coordinate m (in solar masses $M_\odot$) in the central part of the core at $0 \le m \le 2.5$. The bottom panel shows the dimensionless concentrations of matter components $Y_i = n_i/n_b$, where n_b is the concentration of baryons; Y_i are related to commonly used weight fractions X_i as $X_i = A_i Y_i$, where A_i is the mass number of the component. As can be seen, the ^{56}Fe isotope is predominate in the hottest part of the core up to $m \approx 1\,M_\odot$.

4 NEUTRINO GENERATION INSIDE PRE-SN

In this section, we consider various processes of neutrino generation under the pre-supernova conditions described above. First, we

Table 1. Different (anti)neutrino generation processes considered in the present study. The x label denotes three neutrino flavours, i.e. $x = \mathrm{e},\ \mu,\ \tau$.

label	process
EC	$^{56}\mathrm{Fe} + e^- \rightarrow {}^{56}\mathrm{Mn} + \nu_\mathrm{e}$
β^+	$^{56}\mathrm{Fe} \rightarrow {}^{56}\mathrm{Mn} + e^+ + \nu_\mathrm{e}$
PC	$^{56}\mathrm{Fe} + e^+ \rightarrow {}^{56}\mathrm{Co} + \bar{\nu}_\mathrm{e}$
β^-	$^{56}\mathrm{Fe} \rightarrow {}^{56}\mathrm{Co} + e^- + \bar{\nu}_\mathrm{e}$
ND	$^{56}\mathrm{Fe}^* \rightarrow \nu_x + \bar{\nu}_x$
PA	$e^- + e^+ \rightarrow \nu_x + \bar{\nu}_x$
PL	plasmon $\rightarrow \nu_x + \bar{\nu}_x$
PH	$e^- + \gamma \rightarrow e^- + \nu_x + \bar{\nu}_x$
BR	$e^- + (A, Z) \rightarrow e^- + (A, Z) + \nu_x + \bar{\nu}_x$

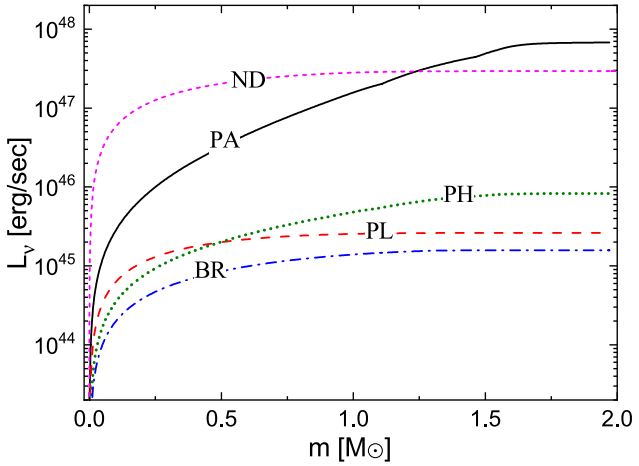

Figure 2. Total (anti)neutrino luminosities inside the central part of the star for the pair production processes listed in Table 1.

describe the generation processes themselves, then we calculate the corresponding neutrino luminosities inside the stellar core, and finally, we determine the spectra of the neutrino flux leaving the star.

4.1 Neutrino processes

In what follows, we will distinguish neutrino processes according to the type of neutrinos they produce. In Table 1, in three rows we collect i) the processes of ν_e generation, ii) the same for $\bar{\nu}_\mathrm{e}$ and iii) $\nu\bar{\nu}$-processes, where neutrinos of all three flavours could be born. Among the latter are the ND pair emission by hot ^{56}Fe, electron–positron pair annihilation (PA), plasmon decay (PL), photo-neutrino production (PH), and bremsstrahlung (BR). We note that neutrinos from the recombination have a luminosity more than four orders of magnitude less than that from other processes and we do not consider them.

Before proceeding with the calculations of luminosities and spectra for (anti)neutrinos of different types, let us find the total neutrino luminosities due to various $\nu\bar{\nu}$ processes listed in Table 1. For this purpose, we use the collection of subroutines by F. X. Timmes[2], who implemented the approximations from Itoh et al. (1996). To compute the neutrino luminosity due to the ND process, we apply the TQRPA method.

Fig. 2 shows the *total* (i.e. ν and $\bar{\nu}$ of all flavours) luminosities in the central part of the star as a function of the mass coordinate m. As

[2]https://cococubed.com/code_pages/nuloss.shtml

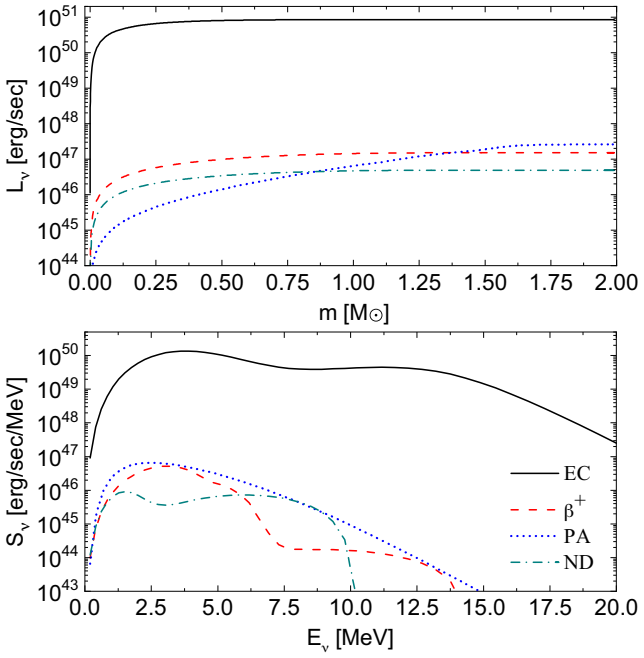

Figure 3. Upper panel: ν_e-type neutrino luminosities as functions of the mass coordinate m. Lower panel: spectrum of ν_e-type neutrinos, leaving the star.

seen from the figure, only PA and ND neutrinos are important under the considered conditions. Therefore, in the subsequent discussion, we account for only these pair production processes. It should be noted that ND neutrinos have the highest luminosity in the very central part of the star, but the growth of their luminosity is almost completely halted after $m \approx 0.5\,\mathrm{M}_\odot$. The reason for this is that the very central part of the star has a sufficiently high temperature $T_9 \approx 9.0$–10.0 to enable the emission of high-energy $\nu\bar{\nu}$-pairs via the ND process. These high-energy pairs are produced by the de-excitation of the thermally excited GT_0 resonance (see fig. 4in Dzhioev et al. 2023 and its discussion). In ^{56}Fe, the GT_0 resonance is located at about 10 MeV and its thermal population rapidly decreases as we move into the colder parts of the star. Because of this, the emission of high-energy (anti)neutrinos due to the ND process stops, which leads to stagnation in the luminosity. In contrast, the luminosity of PA neutrinos continues to grow up to $m \approx 1.7\,\mathrm{M}_\odot$ and ends up being more intense (see Misiaszek, Odrzywołek & Kutschera 2006, where the problem with the PA luminosity and spectrum calculations is discussed).

4.2 ν_e-type neutrino

Now, we are ready to calculate neutrino luminosities and spectra for specified processes. First, let us consider the processes that produce electron-type neutrinos, i.e. EC, β^+, ND, and PA (see Table 1).

In Fig. 3, the ν_e neutrino luminosity $L_\nu[\mathrm{erg\,sec}^{-1}]$ is shown as a function of the mass coordinate in the inner part of a star, $0 \leq m \leq 2$ (upper panel). As is evident from the figure, EC neutrinos are several orders of magnitude more luminous than neutrinos from other processes. Moreover, the luminosity of EC neutrinos greatly exceeds the luminosity of $\bar{\nu}_\mathrm{e}$ and $(\mu,\ \tau)$ (anti)neutrinos produced in various nuclear and thermal processes. Thus, it appears that EC on ^{56}Fe is the dominant energy loss process for

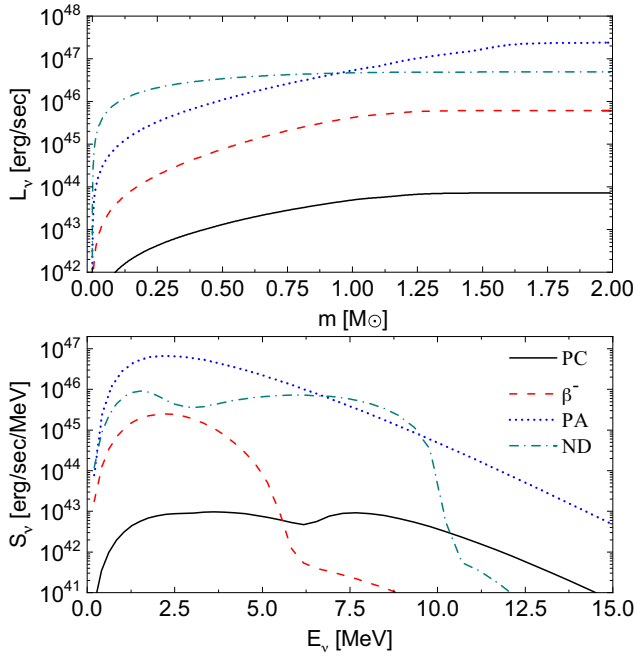

Figure 4. The same as in Fig. 3 but for $\bar{\nu}_e$-type neutrinos.

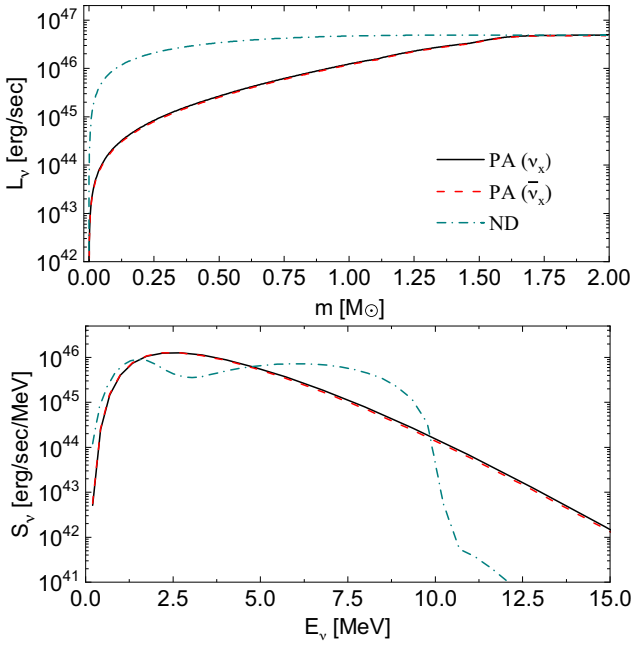

Figure 5. The same as in Fig. 3 but for ν_x- and $\bar{\nu}_x$-type neutrinos, where x stands for μ or τ.

the considered pre-supernovae conditions, and the present study confirms the conclusion made by Fischer, Langanke & Martínez-Pinedo (2013) about the role of electron capture in core-collapse supernovae.

The lower panel of Fig. 3 shows the energy luminosity spectrum S_ν[erg sec^{-1} MeV^{-1}] (which is connected to the total luminosity as $L_\nu = \int S_\nu dE_\nu$) of ν_e neutrinos leaving the star. It is evident that EC neutrinos not only have a much higher total luminosity than ν_e from other processes but also a higher average energy (see the discussion in Section 5).

4.3 $\bar{\nu}_e$-type neutrino

Regardless of the fact that ν_e-type neutrinos, primarily from EC, are the most important energy loss source in a star, $\bar{\nu}_e$ neutrinos are also important. This is due to the fact that most detectors are especially sensitive to the inverse beta-decay reaction initiated namely by $\bar{\nu}_e$ (see the discussion in Section 7).

Fig. 4 shows the same quantities (luminosity and spectrum) as in Fig. 3 but for $\bar{\nu}_e$. As obvious from the figure, the essential difference compared to the previously considered case is that there is no one dominant process that produces the $\bar{\nu}_e$ flux. The PC and β^- contributions are small and, in the very centre of the star, the ND antineutrinos are most luminous. But as discussed above, due to the temperature decrease as we move from the centre and a strong temperature dependence of the ND process, the growth of their luminosity almost stops completely after $m \approx 0.5\,M_\odot$. On the other hand, L_ν from the PA process grows up till $m \approx 1.7\,M_\odot$ and the resultant luminosity is several times higher than that from the ND process. However, while the spectrum of PA antineutrinos is peaked at low energies, $\bar{\nu}_e$ from the ND process have a higher energy peak in the spectrum at $E_\nu \approx 6.0$ MeV, and their luminosity even exceeds the PA luminosity in the energy range $E_\nu \approx 6$–9 MeV. We will discuss the implications of this in Section 7.

4.4 $\nu_{\mu,\tau}$- and $\bar{\nu}_{\mu,\tau}$-type neutrino

Despite the fact that emission of heavy-lepton type (anti)neutrinos has basically no impact on the energy loss during the pre-supernova phase, this process might be important from the point of view of the detection, which is possible due to flavour oscillations. So we have calculated the luminosities and spectra for (μ, τ) (anti)neutrinos as well and put them in Fig. 5.

Referring to the figure, the luminosities and spectra of μ, τ-type neutrinos and antineutrinos produced by the pair annihilation are very close, while for the ND process they are exactly the same. Therefore, further we will not distinguish L_ν, S_ν between $\nu_{\mu,\tau}$ and $\bar{\nu}_{\mu,\tau}$. We also see that the final (i.e. at $m = 2.0\,M_\odot$) PA and ND luminosities are almost the same, but the spectra are quite different. As in the case of $\bar{\nu}_e$, the PA spectrum of (μ, τ) (anti)neutrinos is peaked at low energies, while the ND spectrum has a high-energy peak at $E_\nu \approx 6.0$ MeV. Recall that nuclear de-excitation produces the same spectra for all (anti)neutrino flavours. When Fig. 5 is compared with Fig. 4, it is apparent that production of heavy-lepton flavour (anti)neutrinos in the PA process is lower than that of e-type (anti)neutrinos. This is because pair annihilation into $\nu_e\bar{\nu}_e$ proceeds via both neutral and charged currents, while $\nu_x\bar{\nu}_x$ ($x = \mu$, τ) pairs are produced only via neutral current Z^0 boson exchange (Misiaszek, Odrzywołek & Kutschera 2006). For this reason, the ND process appears to be more important for μ and τ (anti)neutrino production than for ν_e and $\bar{\nu}_e$.

5 CHARACTERISTIC FEATURES OF THE TQRPA METHOD

Before we proceed to discussing the issue of detecting pre-supernova neutrinos on the Earth, let us compare our method with that used in the MESA code. The MESA code is based on the pre-calculated weak-interaction reaction tables (for EC, PC, and $\beta^\pm$ processes), which for ^{56}Fe are obtained applying large-scale shell-model calculations (Langanke & Martínez-Pinedo 2000). In the present study, the electron (anti)neutrino spectra and luminosities from the LSSM

weak-interaction rates are computed on the basis of extended tables[3] by applying the effective q-value method (Langanke, Martínez-Pinedo & Sampaio 2001; Patton, Lunardini & Farmer 2017a). Namely, it is assumed that a weak process on a state in the parent nucleus leads to a single state in the daughter nucleus and the energy difference, q, between the initial and final states is the same for all excited states in the parent nucleus (Brink's hypothesis). Then, for a single nucleus, the neutrino spectra from charge-exchange weak reactions take the form

$$\phi^{\mathrm{EC,PC}}(E_\nu) = N_{\mathrm{EC,PC}} \frac{E_\nu^2 (E_\nu - q)^2}{1 + \exp\left(\dfrac{E_\nu - q \mp \mu_\mathrm{e}}{kT}\right)} \Theta(E_\nu - q - m_\mathrm{e}c^2),$$
$$\phi^{\beta^\pm}(E_\nu) = N_{\beta^\pm} \frac{E_\nu^2 (E_\nu - q)^2}{1 + \exp\left(\dfrac{E_\nu - q \mp \mu_\mathrm{e}}{kT}\right)} \Theta(q - E_\nu - m_\mathrm{e}c^2), \tag{8}$$

where the upper (lower) sign refers to EC and β^+ (PC and β^-) and μ_e is the electron chemical potential. The effective q-value and normalization factors N_i are fitting parameters, and they are adjusted to the average (anti)neutrino energy and weak reaction rates

$$\langle E_{\nu,\bar\nu} \rangle = \frac{\int_0^\infty (\phi^{\mathrm{EC,PC}} + \phi^{\beta^\pm}) E_\nu \, \mathrm{d}E_\nu}{\int_0^\infty (\phi^{\mathrm{EC,PC}} + \phi^{\beta^\pm}) \, \mathrm{d}E_\nu}, \tag{9}$$

$$\lambda^i = \int_0^\infty \phi^i(E_\nu) \, \mathrm{d}E_\nu \quad i = \mathrm{EC,PC}, \beta^\pm. \tag{10}$$

The values of $\langle E_{\nu,\bar\nu} \rangle$ and λ^i are listed in the LSSM rate tabulations for a grid of temperature/density points and can be easily interpolated in between (Fuller, Fowler & Newman 1985). Note that for ^{56}Fe under the considered pre-supernova conditions, the effective q-value method results in a negative q for the ν_e spectrum. This means that according to equation (8), only electron captures contribute to ν_e production in the charge-exchange channel. In contrast, for the $\bar\nu_\mathrm{e}$ spectrum, we have $q > m_\mathrm{e}c^2$, i.e. both PC and β^--decay contribute to $\bar\nu_\mathrm{e}$ emission.

To compute ND (anti)neutrino spectra within the shell-model method, we use the ground-state GT_0 strength distribution $S_{\mathrm{GT}_0}(E)$ for ^{56}Fe derived from the LSSM calculations (see fig. 1 in Sampaio et al. 2002). Then, we apply the same method as in Fischer, Langanke & Martínez-Pinedo (2013) to obtain the GT_0 strength function for pair emission. Namely, adopting Brink's hypothesis and exploiting the detailed balance relation (6), we get

$$\phi^{\mathrm{ND}}(E_\nu) = \frac{G_\mathrm{F}^2 g_A^2}{2\pi^3 \hbar^7 c^6} E_\nu^2 \int_{E_\nu}^\infty S_{\mathrm{GT}_0}(E) \exp\left(-\frac{E}{kT}\right) (E - E_\nu)^2 \, \mathrm{d}E. \tag{11}$$

Combining this expression with the effective q-value method for charge-changing processes, we obtain the LSSM (anti)neutrino spectra from nuclear processes.

In Fig. 6, we compare the TQRPA and LSSM (anti)neutrino energy luminosity spectra from nuclear processes integrated over the emission region $m \leq 2\,\mathrm{M}_\odot$. Focusing on the upper panel of the figure, we notice that both the TQRPA and LSSM calculations give a low-energy peak in the ν_e spectrum at $E_\nu \approx 4.0$ MeV. In both methods, EC dominates ν_e production, and the observed low-energy peak is mainly caused by the GT_+ resonance excitation. The TQRPA approach also produces a second higher energy peak, which makes

[3] https://theory.gsi.de/~gmartine/rates/

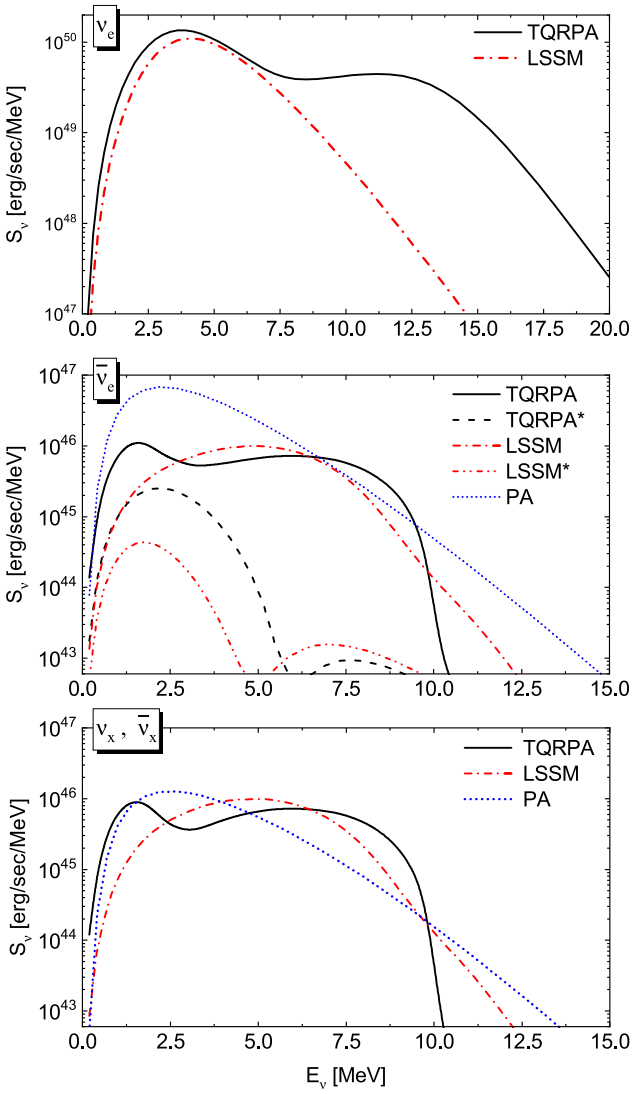

Figure 6. Comparison of the TQRPA and LSSM (anti)neutrino spectra from nuclear processes. In both methods, the ν_e spectra shown in the upper panel are determined almost entirely by the electron capture (see Fig. 3). In the middle panel, labels 'TQRPA' and 'LSSM' represent the $\bar\nu_\mathrm{e}$ spectra that include contributions from PC, β^--decay, and ND, while spectra obtained without the ND contribution are marked as 'TQRPA∗' and 'LSSM∗'. The ν_x and $\bar\nu_x$ ($x = \mu, \tau$) spectra from the ND process are the same in the lower panel. In the middle and lower panels, we also show the spectra from the pair annihilation thermal process.

the spectrum harder. This high-energy peak correspond to ν_e emitted after downward negative-energy transitions from thermally excited states. We would like to emphasize that the absence of the second peak in the LSSM spectrum is the result of the effective q-value approximation. In the LSSM calculations of stellar weak-interaction rates, downward transitions are taken into account using the back-resonance method (Langanke & Martínez-Pinedo 2000), and they produce a high-energy peak in the neutrino spectrum (see e.g. fig. 2 in Langanke, Martínez-Pinedo & Sampaio 2001).

The role of the ND process in the $\bar\nu_\mathrm{e}$ spectrum is depicted in the middle panel of Fig. 6, where the TQRPA and LSSM spectra with and without the ND contribution are compared with the PA spectrum. As illustrated, the TQRPA and LSSM spectra without the ND contribution have a double-bump structure, reflecting the

contribution of PC and β^--decay. Both methods predict that in the absence of the ND process, emission of pre-supernova $\bar{\nu}_e$ is entirely dominated by pair annihilation. Taking nuclear de-excitation into account increases the role of nuclear processes in $\bar{\nu}_e$ emission. In both methods, the high-energy ND contribution around $E_\nu \approx 7$–9 MeV is comparable or even exceeds the PA contribution. For heavy-lepton flavour (anti)neutrino emission, the role of the ND process is even more important (see the lower panel of Fig. 6).

Comparing the ND spectra from the TQRPA and LSSM calculations, we notice that the LSSM produces a single-peak spectrum, which is different from the double-peak spectrum produced by the TQRPA. In both methods, the high-energy peak corresponds to (ant)neutrinos emitted via de-excitation of the GT_0 resonance. The TQRPA calculations of the GT_0 strength distribution in ^{56}Fe predict a somewhat higher centroid energy of the GT_0 resonance as compared to the shell-model strength distribution (see fig. 1 in Dzhioev et al. 2016). As a result, the high-energy peak in the TQRPA spectrum is slightly shifted to higher energies. The appearance of a low-energy peak in the TQRPA spectrum is related to thermally unblocked low-energy GT_0 transitions, which, owing to the detailed balance principle, significantly increase the strength of inverse negative-energy transitions (Dzhioev et al. 2016). Due to the application of Brink's hypothesis, no such transitions appear in the GT_0 strength distribution obtained from the ground-state LSSM calculations. For this reason, within the TRQPA, the average energy of emitted ND (anti)neutrinos ($\langle\mathcal{E}^{\nu\bar{\nu}}\rangle_{\rm TQRPA} = 2.97$ MeV) is lower than that obtained from the LSSM calculations ($\langle\mathcal{E}^{\nu\bar{\nu}}\rangle_{\rm LSSM} = 4.07$ MeV). However, the luminosities of ND (anti)neutrinos in both methods are nearly the same ($L^{\nu\bar{\nu}}_{\rm TQRPA} = 4.9$, $L^{\nu\bar{\nu}}_{\rm LSSM} = 4.6$). It is also interesting to note that $\langle\mathcal{E}^{\nu\bar{\nu}}\rangle_{\rm TQRPA}$ is close to the values of $\langle\mathcal{E}^{\nu\bar{\nu}}\rangle$ obtained in Fischer, Langanke & Martínez-Pinedo (2013) (see Table II) at $T = 0.7$ and 1.0 MeV.

The similarities and differences between the expected total (i.e. nuclear plus thermal) TQRPA and LSSM spectra as well as the role of the ND process in the pre-supernova (anti)neutrino emission are summarized in Fig. 7. The comparison between the TQRPA and LSSM spectra for ν_e and the discussion of the reasons for their differences has been made above. Here, we just mention that within the TQRPA, the energy luminosity $L_{\nu_e} = \int S_{\nu_e}(E_\nu)\,dE_\nu$ is about twice larger than that predicted by the LSSM. The reasons for this are discussed below.

As for the total $\bar{\nu}_e$ spectra, we remind that in both methods the role of PC and β^--decay is negligible and without the ND contribution the spectra are dominated by the PA process. As shown in the middle panel of Fig. 7, the ND process only slightly enhances the emission of low-energy $\bar{\nu}_e$, but at higher energies $E_\nu = 7$–9 MeV, its contribution is comparable or even bigger than the PA one. It should be emphasized that the increased role of the ND process in the emission of high-energy $\bar{\nu}_e$ is confirmed by both the TQRPA and LSSM methods.

Referring to the lower panel of Fig. 7, the dominating role of ND (anti)neutrinos in the $\nu_{\mu,\tau}$ and $\bar{\nu}_{\mu,\tau}$ spectra is predicted by both the TQRPA and LSSM calculations, and both methods demonstrate the increased contribution of the ND process to the emission of high-energy (μ, τ) (anti)neutrinos. Thus, the present study generalizes the results of Fischer, Langanke & Martínez-Pinedo (2013), and we can conclude that nuclear de-excitation via $\nu\bar{\nu}$-pair emission might be a leading source for the production of heavy-lepton type (anti)neutrinos not only during the collapse phase but also during the pre-supernova phase. Once again, we stress that this result is confirmed by both TQRPA and LSSM calculations. Considering that detection of $\bar{\nu}_e$ is the main detection channel and taking into account

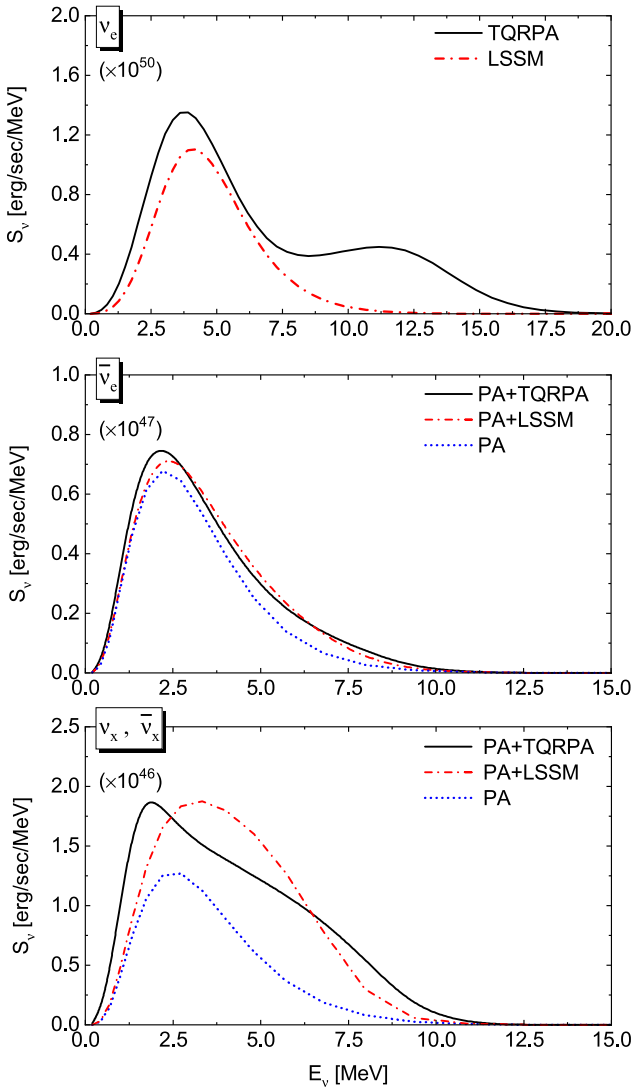

Figure 7. Total (i.e. nuclear plus thermal) (anti)neutrino spectra obtained from the TQRPA and LSSM calculations. For ν_e neutrinos only electron captures are important and contributions from other nuclear and thermal processes are negligible. Note also that the $\bar{\nu}_e$ spectra without the ND contribution can be considered with good accuracy as the PA ones (see the middle panel in Fig. 6). The neutrino spectra should be multiplied by the number shown in parenthesis.

that flavour oscillations can swap the $\bar{\nu}_e$ and $\bar{\nu}_{\mu,\tau}$ spectra, it is clear that this result might be important for experiments. We will return to this problem in the next two sections.

Table 2 lists the average (anti)neutrino energies $\langle\mathcal{E}_\nu\rangle = \int S_\nu(E)\,dE / \int S_\nu(E)E^{-1}\,dE$ and the luminosities $L_\nu = \int S_\nu(E)\,dE$ computed from the total spectra shown in Fig. 7. As seen from the table, both the TQRPA and LSSM calculations predict that at pre-supernova phase, the most luminous and energetic are electron neutrinos. In both methods, the ND process increases the energy luminosities $L_{\bar{\nu}_e,\,\nu_x,\bar{\nu}_x}$ $(x = \mu,\,\tau)$, and this effect is significant for heavy-lepton type (anti)neutrinos. The ND process also slightly increases the average energy for $\bar{\nu}_e$, ν_x, and $\bar{\nu}_x$. This increase is most pronounced for $\langle\mathcal{E}_{\nu_x,\bar{\nu}_x}\rangle_{\rm LSSM}$. In the TQRPA, the ND process simultaneously enhances both the low- and high-energy parts of the spectrum (see the lower panel of Fig. 7), which is why $\langle\mathcal{E}_{\nu_x,\bar{\nu}_x}\rangle_{\rm TQRPA}$ remains almost unchanged.

Table 2. Average energy $\langle \mathcal{E}_\nu \rangle$ (in MeV) and luminosity L_ν (in erg sec^{-1}) of the (anti)neutrinos produced by all processes listed in Table 1, for the considered pre-supernova model. Columns marked with a star symbol show data computed without the ND contribution.

	TQRPA	TQRPA∗	LSSM	LSSM∗
$\langle \mathcal{E}_{\nu_e} \rangle$	4.68	4.68	4.04	4.04
L_{ν_e}	8.52×10^{50}	8.52×10^{50}	4.67×10^{50}	4.67×10^{50}
$\langle \mathcal{E}_{\bar{\nu}_e} \rangle$	2.49	2.41	2.58	2.41
$L_{\bar{\nu}_e}$	2.93×10^{47}	2.44×10^{47}	2.85×10^{47}	2.39×10^{47}
$\langle \mathcal{E}_{\nu_x, \bar{\nu}_x} \rangle$	2.82	2.68	3.21	2.68
$L_{\nu_x, \bar{\nu}_x}$	9.78×10^{46}	4.88×10^{46}	9.50×10^{46}	4.88×10^{46}

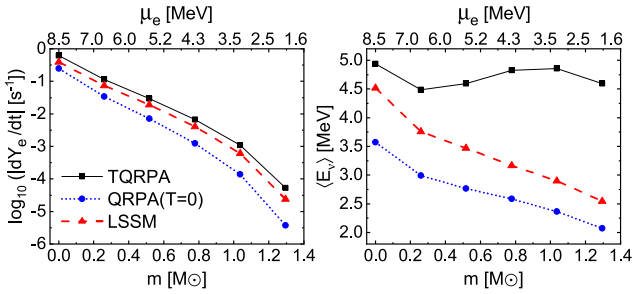

Figure 8. Electron capture rate $|dY_e/dt| = Y_{^{56}Fe} \lambda^{EC}$ (left-hand panel) and average energy $\langle E_\nu \rangle$ of emitted EC neutrinos (right-hand panel) as functions of the mass coordinate. The TQRPA results are compared with the LSSM calculations. To demonstrate the importance of thermal effects, we also show the results of the QRPA calculations, which correspond to a cold ($T = 0$) ^{56}Fe nucleus. The upper x-axis shows the chemical potential μ_e.

The TQRPA and LSSM results in Table 2 are in reasonable agreement with each other except the electron neutrino luminosity L_{ν_e}. Namely, the TQRPA result is about twice the luminosity calculated from the LSSM. We remind that in both methods, electron captures on ^{56}Fe are the main source of ν_e. It must be emphasized that the L_{ν_e} value obtained in the LSSM is not a result of the q-value approximation, but it can be calculated directly from the LSSM weak-interaction rate tables.[4] To understand the reason for the discrepancy, we note two facts. First, at pre-supernova temperatures, $T_9 \approx 2$–10, the TQRPA rates for electron capture by ^{56}Fe generally exceed the shell-model ones (see fig. 3 in Dzhioev, Vdovin & Stoyanov 2019). A comparison of the TQRPA and LSSM electron capture rates $|dY_e/dt| = Y_{^{56}Fe} \lambda^{EC}$ along the mass coordinate, shown in the left-hand panel of Fig. 8, confirms this observation. A detailed analysis performed in Dzhioev et al. (2010) reveals that this disagreement stems from a larger strength of thermally unblocked low- and negative-energy Gamow-Teller transitions predicted by the TQRPA. Second, a larger strength of thermally unblocked low- and negative-energy transitions favours the emission of high-energy EC neutrinos. This can be clearly seen (see the right-hand panel of Fig. 8) if we compare the TQRPA and LSSM average energy $\langle E_\nu \rangle$ of emitted EC neutrinos. According to the LSSM calculations, $\langle E_\nu \rangle$ is significantly lowered when we move from the centre of the star decreasing the chemical potential μ_e, whereas it varies rather weakly around $\langle E_\nu \rangle \approx$ 4.7 MeV within the TQRPA. This stability is a result of the increased fraction of high-energy neutrinos emitted due to thermally unblocked transitions, which compensate for the decrease in available electron energy. It is clear that both these facts enhance the EC neutrino luminosity.

To demonstrate the importance of thermal effects, we compute electron capture rates and average neutrino energies within the QRPA, i.e. for a cold nucleus ^{56}Fe. Referring to Fig. 8, without thermal effects, i.e. without thermally unblocked low- and negative-energy GT$_+$ transitions, EC rates and average neutrino energies are significantly smaller than the one obtained in finite temperature TQRPA and LSSM calculations. We also see that the importance of thermal effects increases as the chemical potential μ_e reduces.

Obviously, due to larger electron capture rates, the core should radiate more energy away by neutrino emission, keeping the core on a trajectory with lower temperature and entropy. Moreover, larger electron capture rates predicted by the TQRPA for iron-group nuclei should basically result in a faster deleptonization of the progenitor star core at the pre-collapse and early collapse phases. We note, however, that the difference between the TQRPA and LSSM rates is much smaller than that (Langanke & Martínez-Pinedo 2000) between the LSSM rates and electron capture rates estimated by Fuller, Fowler, and Newman on the basis of the independent particle model (Fuller, Fowler & Newman 1982). Besides, a larger strength of thermally unblocked negative-energy transitions accelerates, the total β^--decay rate, which, for a certain range of electron-to-baryon ratios Y_e, can exceed the electron capture rate (Martínez-Pinedo, Langanke & Dean 2000) and counteracts the reduction of Y_e. Anyway, definite conclusions about the influence of the TQRPA rates on (pre-)supernova models might be drawn only on the basis (pre)-supernova computer simulations employing these new rates.

6 OSCILLATIONS

In principle, the calculated spectra of neutrinos and antineutrinos are not yet sufficient to estimate the effect produced in the Earth's detectors. In fact, we should also take into account the influence of neutrino flavour oscillations. To do this, we will follow a simple approach (Kato et al. 2015), which allows us to at least qualitatively assess the impact of this effect. We will focus on $\bar{\nu}_e$-type neutrinos, as being of primary interest in terms of detection (see below Section 7). So we will assume that the electron antineutrino spectrum after oscillation can be written as

$$S_{\bar{\nu}_e} = p S^0_{\bar{\nu}_e} + (1-p) S^0_{\bar{\nu}_x}, \quad (12)$$

where index 0 stands for the original unoscillated spectra and $x = \mu$ or τ. In equation (12), the quantity p is the survival probability, which is connected to the mixing parameters as $p = \cos^2\theta_{12} \cos^2\theta_{13} \approx 0.676$ for the normal hierarchy (NH) and $p = \sin^2\theta_{13} \approx 0.024$ for the inverted hierarchy (IH) (see e.g. Kolupaeva et al. 2023). Thus, the NH provides moderate mixing while the IH almost suppresses the original $\bar{\nu}_e$ flux and replaces it by that for $\bar{\nu}_\mu$ or $\bar{\nu}_\tau$, both of which have the same spectrum. Let us remind that according to Table 1 and the discussion in Section 4, the original $\bar{\nu}_e$ flux is produced by the PC, β^-, PA, and ND processes, while the $\bar{\nu}_{\mu,\tau}$ flux is formed in the last two processes.

In Fig. 9, we present the total (nuclear plus thermal) $\bar{\nu}_e$ spectra for the normal and inverted hierarchies computed within the TQRPA and LSSM approaches and compare them with the unoscillated spectra. On each plot, we also show the ND contribution which does not depend on oscillations since $S^{0,ND}_{\bar{\nu}_e} = S^{0,ND}_{\bar{\nu}_x}$. From the TQRPA and LSSM plots, one can see that NH oscillations have a small effect on the shape of the original unoscillated spectrum and just decrease its absolute value. Therefore, the average energy of $\bar{\nu}_e$ remains almost unchanged (see Table 2) while their total luminosity $L_{\bar{\nu}_e}$ is suppressed

[4] https://theory.gsi.de/~gmartine/rates/

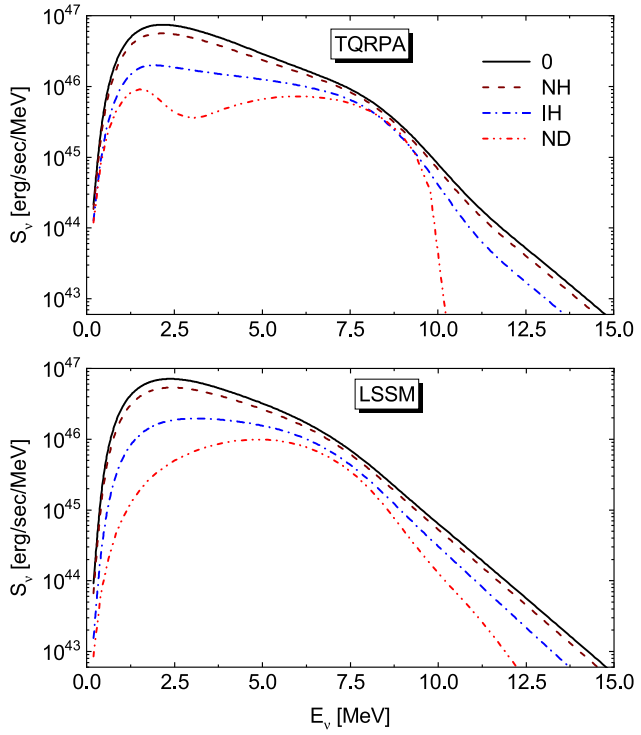

Figure 9. The total $\bar{\nu}_e$ spectra obtained with the normal (NH) and inverted (IH) hierarchy are compared with the original unoscillated spectrum (0). On each plot, we also show the ND contribution to the spectra.

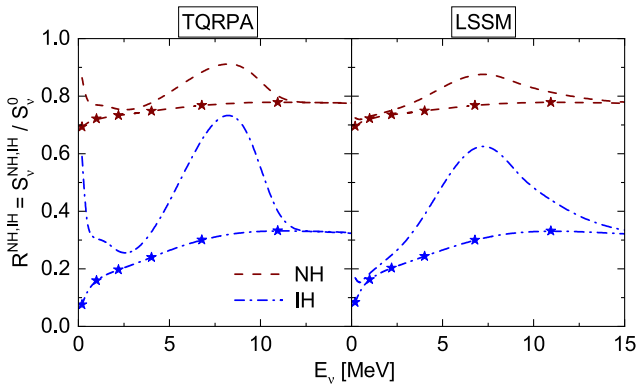

Figure 10. The ratio $R^{\rm NH,\,IH}$ of the spectra obtained with the normal and inverted hierarchies to the unoscillated one. The ratios computed without the ND contribution are marked with a star symbol.

by a factor of ∼0.7. In contrast, replacing the original $\bar{\nu}_e$ flux by the $\bar{\nu}_x$, one caused by IH oscillations results in a significant suppression of the spectrum except the energy range, where the ND contribution dominates. As a result, $L_{\bar{\nu}_e}$ is lowered by a factor of more than three, while $\langle\mathcal{E}_{\bar{\nu}_e}\rangle_{\rm LSSM}$ rises from from 2.6 to 3.2 MeV, and $\langle\mathcal{E}_{\bar{\nu}_e}\rangle_{\rm TQRPA}$ is practically unchanged.

To demonstrate the energy dependence of the $\bar{\nu}_e$ spectrum suppression due to oscillations in Fig. 10, we plot the ratio $R^{\rm NH,IH}(E_\nu) = S^{\rm NH,IH}_{\bar{\nu}_e}(E_\nu)/S^0_{\bar{\nu}_e}(E_\nu)$. Referring to the figure, without the ND contribution, the ratio $R^{\rm NH}$ is close to the survival probability $p = 0.676$, while the value of $R^{\rm IH}$ is determined by the ratio $S^{0,\rm PA}_{\bar{\nu}_x}/S^{0,\rm PA}_{\bar{\nu}_e}$. The latter increases from 0.1 at low energies up to 0.3 at $E_\nu \approx 15$ MeV. The inclusion of the ND process changes a monotonic energy dependence of $R^{\rm NH,\,IH}$. Namely, both the TQRPA and LSSM calculations demonstrate that for high-energy ($E_\nu \approx$ 5–10 MeV) antineutrinos, the ND process reduces spectrum suppression and this effect is most pronounced for IH oscillations. Within the TRQPA approach, the ND process also increases the fraction of low-energy neutrinos in the oscillated $\bar{\nu}_e$ spectrum, which, as discussed earlier in Section 5, is due to temperature-induced increase in the strength of low-energy GT_0 transitions in ^{56}Fe.

7 DETECTION

The dominant detection process for electron antineutrinos from (pre-)supernova is the inverse beta-decay:

$$\bar{\nu}_e + p \to n + e^+. \tag{13}$$

Of course, other reactions can be important as well (see e.g. Manukovskiy et al. 2022), but here we will focus on the most standard one. The cross-section of (13) can be estimated as (see e.g. Odrzywolek, Misiaszek & Kutschera 2004a)

$$\sigma_{\rm IBD} \sim p_{e^+} E_{e^+}, \tag{14}$$

where $E_{e^+} = E_{\bar{\nu}} - (m_{\rm n} - m_{\rm p})c^2$ is the emitted positron energy and p_{e^+} is its momentum. So the minimum threshold energy required to induce this reaction is $E^{\rm min}_{\bar{\nu}} = (m_{\rm n} - m_{\rm p} + m_e)c^2 \approx 1.8$ MeV. If the detector employed has the detection efficiency 100 per cent above the threshold $E_{\rm th} \geq 1.8$ MeV, then the number of detected electron antineutrinos with the energy spectrum $S(E_{\bar{\nu}})$ is expressed as

$$N(E_{\rm th}) \sim \int_{E_{\rm th}}^{\infty} \sigma_{\rm IBD}(E_{\bar{\nu}}) S(E_{\bar{\nu}}) \frac{{\rm d}E_{\bar{\nu}}}{E_{\bar{\nu}}}. \tag{15}$$

Applying this relation and using the TQRPA and LSSM spectra shown in Fig. 9, we constructed Fig. 11 to compare three cases: NH, IH, and unoscillated one.

In Fig. 11, with the solid curves with filled symbols, we denote a relative number of events in the detector, $N(E_{\rm th})/N_0$, as a function of the threshold energy. Here, the normalization constant N_0 is $N(E_{\rm th} = 1.8\,{\rm MeV})$ for the unoscillated TQRPA spectrum. We note that $N_0^{\rm TQRPA}$ and $N_0^{\rm LSSM}$ are rather close to each other. As indicated in the figure, NH oscillations lead to a moderate reduction of the $N(E_{\rm th})/N_0$ ratio, whereas IH oscillations reduce the number of detected events by about half. Besides, the ratio $N(E_{\rm th})/N_0$ demonstrates the importance of the detector's threshold parameter $E_{\rm th}$ and how drastically it can affect the number of registered pre-supernova $\bar{\nu}_e$. For example, a rather moderate value of $E_{\rm th} \approx 5$ MeV reduces the number of registered events by almost half.

In order to show the effect of the ND process on neutrino detection in Fig. 11, we also plot with the dashed curves with empty symbols the quantity

$$D(E_{\rm th}) = \left(1 - \frac{N^{\rm ND}(E_{\rm th})}{N(E_{\rm th})}\right)^{-1}, \tag{16}$$

which is a detection rate enhancement factor due to ND neutrinos (right axes). As expected, ND neutrinos play an important role in the case of IH oscillations. Namely, for $E_{\rm th} \approx$ 5–8 MeV, they enhance the TQRPA and LSSM detection rates by factors 5.5 and 3.5, respectively. At low threshold energies, the enhancement factor is $D \approx 3.0$. An increase in the survival probability p diminishes the role of ND neutrinos, but even in the case of unoscillated spectra, they still contribute substantially to $\bar{\nu}_e$ neutrino detection for $E_{\rm th} \approx$ 5–8 MeV.

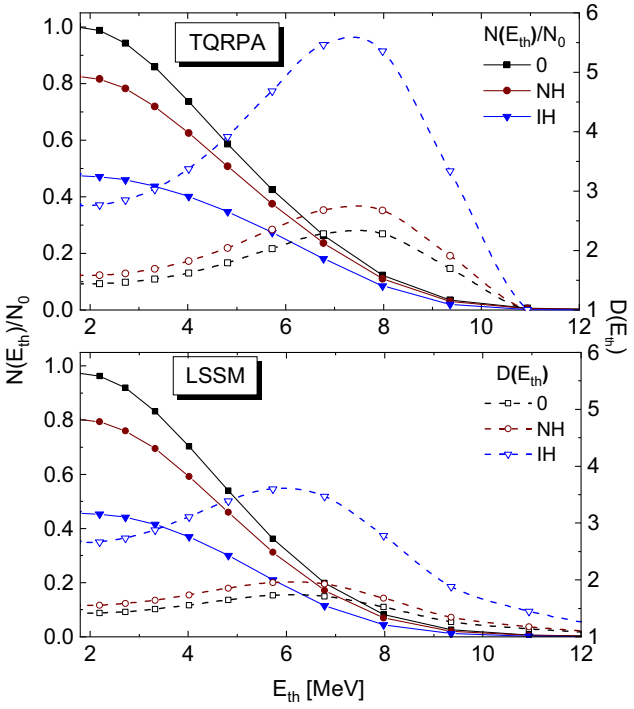

Figure 11. The relative number $N(E_{\rm th})/N_0$ of events in the detector and the detection rate enhancement factor $D(E_{\rm th})$ as a function of the threshold energy $E_{\rm th}$.

Thus, we can conclude that from the viewpoint of detection of pre-supernova electron antineutrinos, the neutral-current de-excitation of ^{56}Fe is an important process especially in the moments immediately preceding the collapse when the core temperature is high enough for the thermal population of the GT_0 resonance.

8 SUMMARY AND PERSPECTIVES

Let us summarize the main results of the presented research. With the TQRPA approach, we are able to take into account thermal effects, which influence various nuclear weak-interaction processes contributing to (anti)neutrino generation under the conditions characteristic for a hot (pre-)supernova matter. We focus our attention on (anti)neutrino production by a hot ^{56}Fe, which dominates the isotopic composition of the stellar core at the onset of the collapse. The realistic pre-supernova profile we use was obtained with the help of the famous MESA evolutionary code. In accordance with our previous estimates (Dzhioev et al. 2023), we have found that the TQRPA approach produces not only a higher energy luminosity of electron neutrinos (mainly born in the EC process), compared to a more conventional LSSM approach, but also a harder neutrino spectrum as compared with those produced with the effective q-value approximation. Both these effects are due to a larger strength of low- and negative-energy GT_+ transitions in the thermally excited ^{56}Fe predicted by the TQRPA.

We also have found that the nuclear neutral-current de-excitation process via $\nu\bar{\nu}$-pair emission is at least as important as the electron-positron pair annihilation in the context of the electron antineutrino generation. Our calculations of $\bar{\nu}_e$ spectra based on the TQRPA and LSSM distributions of the GT_0 strength in ^{56}Fe have shown that, although $\bar{\nu}_e$ from the ND process have a lower total luminosity compared to the PA process, their luminosity in the high-energy region $E_\nu = 7$–9 MeV is comparable or even exceeds the PA contribution. Moreover, both the TQRPA and LSSM calculations predict that the ND process is crucial for generation of heavy-lepton flavour (anti)neutrinos under pre-supernova conditions. The latter is of extreme importance because of the problem of pre-supernova neutrino registration by the Earth's detectors. We have also explored the effect of neutrino oscillations and found that ND antineutrinos are important in all cases, but especially in the case of the inverted mass hierarchy when they increase the detection rate by several times.

The main goal of the present study is to draw attention to the importance of the careful treatment of neutrino processes with hot nuclei. Our research can be continued and extended in several aspects. First, it is interesting to study within the TQRPA, the effects of nuclear composition on the neutrino luminosities and spectra. For example, according to Patton et al. (2017b), there is no one dominating nucleus in the centre of the star but rather a bunch of iron-group nuclei such as $^{50-51}$Ti, ^{54}Cr etc. Probably this is due to a different and more extended nuclear reaction network than the one we use. We are planning to address this issue in forthcoming studies.

In addition, the diversity of pre-supernovae may be caused by another factor: a pre-supernova may be part of a close binary system with mass exchange (Laplace et al. 2021), which can lead to significant differences in stellar profiles. And it should be remembered that not only a core-collapse supernova but also a type Ia thermonuclear supernova (Odrzywolek & Plewa 2011) can be a source of neutrinos that can be detected the on the Earth.

ACKNOWLEDGEMENTS

AY and NDB are grateful to S.I. Blinnikov for useful discussions on neutrino spectra from supernova progenitors on the late stages of their evolution. AY thanks RSF 22-12-00103 grant for support. All authors thank the anonymous reviewer for constructive comments and important suggestions that helped improve this manuscript.

DATA AVAILABILITY

Data generated from computations are reported in the body of the paper. Additional data can be made available upon reasonable request.

REFERENCES

Alekseev E. N., Alekseeva L. N., Volchenko V. I., Krivosheina I. V., 1987, Sov. J. Exp. Theor. Phys. Lett., 45, 589
Bionta R. M. et al., 1987, Phys. Rev. Lett., 58, 1494
Caurier E., Langanke K., Martínez-Pinedo G., Nowacki F., 1999, Nucl. Phys. A, 653, 439
Caurier E., Martínez-Pinedo G., Nowacki F., Poves A., Zuker A. P., 2005, Rev. Mod. Phys., 77, 427
Dzhioev A. A., Vdovin A. I., 2022a, Phys. Part. Nuclei., 53, 885
Dzhioev A., Vdovin A. I., 2022b, Phys. Part. Nuclei., 53, 939
Dzhioev A. A., Vdovin A. I., 2022c, Phys. Part. Nuclei., 53, 1051
Dzhioev A. A., Vdovin A. I., Ponomarev V. Y., Wambach J., Langanke K., Martínez-Pinedo G., 2010, Phys. Rev. C, 81, 015804
Dzhioev A. A., Vdovin A. I., Martínez-Pinedo G., Wambach J., Stoyanov C., 2016, Phys. Rev. C, 94, 015805
Dzhioev A. A., Vdovin A. I., Stoyanov C., 2019, Phys. Rev. C, 100, 025801
Dzhioev A. A., Langanke K., Martínez-Pinedo G., Vdovin A. I., Stoyanov C., 2020, Phys. Rev. C, 101, 025805
Dzhioev A. A., Yudin A. V., Dunina-Barkovskaya N. V., Vdovin A. I., 2023, Particles, 6, 682
Farmer R., Fields C. E., Petermann I., Dessart L., Cantiello M., Paxton B., Timmes F. X., 2016, ApJS, 227, 22

Fischer T., Langanke K., Martínez-Pinedo G., 2013, Phys. Rev. C, 88, 065804
Fuller G. M., Fowler W. A., Newman M. J., 1982, ApJ, 252, 715
Fuller G. M., Fowler W. A., Newman M. J., 1985, ApJ, 293, 1
Hirata K. et al., 1987, Phys. Rev. Lett., 58, 1490
Itoh N., Hayashi H., Nishikawa A., Kohyama Y., 1996, ApJS, 102, 411
Kato C., Delfan Azari M., Yamada S., Takahashi K., Umeda H., Yoshida T., Ishidoshiro K., 2015, ApJ, 808, 168
Kato C., Nagakura H., Furusawa S., Takahashi K., Umeda H., Yoshida T., Ishidoshiro K., Yamada S., 2017, ApJ, 848, 48
Kolupaeva L., Gonchar M., Ol'shevskii A., Samoylov O., 2023, Phys. Usp., 66, 753
Kondratyev V. N., Dzhioev A. A., Vdovin A. I., Cherubini S., Baldo M., 2019, Phys. Rev. C, 100, 045802
Kutschera M., Odrzywołek A., Misiaszek M., 2009, Acta Physica Polonica B, 40, 3063
Langanke K., Martínez-Pinedo G., 2000, Nucl. Phys. A, 673, 481
Langanke K., Martínez-Pinedo G., Sampaio J. M., 2001, Phys. Rev. C, 64, 055801
Laplace E., Justham S., Renzo M., Götberg Y., Farmer R., Vartanyan D., de Mink S. E., 2021, A&A, 656, A58
Manukovskiy K. V., Yudin A. V., Agafonova N. Y., Malgin A. S., Ryazhskaya O. G., 2022, Sov. J. Exp. Theor. Phys., 134, 277
Martínez-Pinedo G., Langanke K., Dean D. J., 2000, ApJS, 126, 493
Misch G. W., Fuller G. M., 2016, Phys. Rev. C, 94, 055808
Misiaszek M., Odrzywołek A., Kutschera M., 2006, Phys. Rev. D, 74, 043006
Odrzywolek A., Heger A., 2010, Acta Phys. Polon. B, 41, 1611
Odrzywolek A., Plewa T., 2011, A&A, 529, A156
Odrzywolek A., Misiaszek M., Kutschera M., 2004a, Astropart. Phys., 21, 303
Odrzywolek A., Misiaszek M., Kutschera M., 2004b, Acta Physica Polonica B, 35, 1981
Patton K. M., Lunardini C., Farmer R. J., 2017a, ApJ, 840, 2
Patton K. M., Lunardini C., Farmer R. J., Timmes F. X., 2017b, ApJ, 851, 6
Paxton B. et al., 2015, ApJS, 220, 15
Ryazhskaya O. G., 2006, Physics Uspekhi, 49, 1017
Sampaio J., Langanke K., Martinez-Pinedo G., Dean D., 2002, Physics Letters B, 529, 19
Weaver T. A., Zimmerman G. B., Woosley S. E., 1978, ApJ, 225, 1021

This paper has been typeset from a TEX/LATEX file prepared by the author.